Polymer(Korea), Vol. 41, No. 2, pp. 250-259 (2017)
https://doi.org/10.7317/pk.2017.41.2.250

ISSN 0379-153X(Print)
ISSN 2234-8077(Online)

PVDF/FKM 블렌드의 경화에 따른 열, 인장 및 동적 기계적 성질

Mojtaba Deilamy Moezzi, Mohammad Karrabi†, and Yousef Jahani
Iran Polymer and Petrochemical Institute
(2016년 8월 30일 접수, 2016년 10월 5일 수정, 2016년 11월 14일 채택)

Thermal Tensile, and Dynamic Mechanical Properties of PVDF/FKM Blends in Different Curing Systems

Mojtaba Deilamy Moezzi, Mohammad Karrabi†, and Yousef Jahani
Iran Polymer and Petrochemical Institute P.O. Box: 14965/115, Tehran, I.R. Iran
(Received August 30, 2016; Revised October 5, 2016; Accepted November 14, 2016)

Abstract: Blends of poly(vinylidene fluoride) (PVDF) and fluororubber (FKM) were prepared in an internal mixer by dynamic vulcanization. The effect of FKM, with and without curing system, was studied with respect to the properties of the PVDF/FKM blends. The tensile test showed that the tensile strength and modulus decreased after blending but the elongation-at-break naturally increased because of the presence of rubber in PVDF matrix. The differential scanning calorimetry (DSC) test gave good indications of improved state of miscibility in most blend ratios. The increase of FKM content showed a favorable tendency of PVDF component toward crystallization. The incorporation of FKM as a co-blend improved the thermal stability of PVDF, and the temperature at 10% weight loss of the blends increased. This was confirmed by one value of glass transition temperature obtained from DMTA test, which indicated two different values for pure polymers. The rheological tests showed that the complex viscosity and storage modulus of the blends increased with increasing frequency.

Keywords: poly(vinylidene fluoride), fluororubber, blends, dynamic vulcanization, thermal analysis.

Introduction

The blending of polymers is often a quick and cost effective way to achieve the desired properties of materials which is drawing increasing attention from academia and industry.[1,2] There have been many attempts made to produce new materials from polymer blends because a polymer mixture is much easier to prepare than a new polymer to be synthesized.[3,4] In order to improve the properties of the blends, for example in a plastic/elastomer blend system, vulcanization of the elastomer phase is a useful method to reduce the size of the phase domains, enhancing interfacial adhesion between the two phases and stabilizing the morphology against phase coarsening in the solid state.[5-7] Poly(vinylidene fluoride) (PVDF) polymer is a plastic engineering material of fluorine family. PVDF is widely used in chemical and electrical industries due to their need for materials of high purity, resistance to solvents, acids, bases, heat and low smoke generation, easy melting of fluorine polymers (above 180 °C), high resistance to abrasion and chemicals, and agreeable to the piezoelectric properties of high dielectric and high throughput. PVDF is a semi-crystalline polymer that has the ability to mix with many polymers.[8,9] It has found widespread industrial applications including electronics and has attracted much research interest.[10,11]

Fluoroelastomers (FKM) are a class of synthetic rubber which provide high levels of resistance to heat, oil and chemicals, while providing useful service life above 200 °C. FKM is a collective family of fluoropolymer rubbers and not as a single entity. FKM elastomers can be classified by their fluorine content of 66, 68 or 70% respectively, FKM with higher fluorine content exhibit higher fluid resistance.[12] The outstanding heat stability and excellent oil resistance of these materials are due to the high ratio of fluorine to hydrogen, the strength of the carbon-fluorine bond and the absence of unsaturation.[13,14]

PVDF and FKM have relatively similar physical properties. As one of the special functional fluoroplastics, PVDF has been

†To whom correspondence should be addressed.
E-mail: M.Karabi@ippi.ac.ir

widely studied owing to its remarkable thermal stability, mechanical properties, piezoelectric and pyroelectric qualities, in combination with good resistance to UV irradiation, high temperatures and aggressive chemicals.[15] Dynamic vulcanization is a special process of mixing a thermoplastics and an elastomer to be cross-linked under dynamic conditions. High shear rate above the melting temperature of a thermoplastics and sufficiently high temperature are employed to activate and complete the vulcanization process. Finally, a fine dispersion of the elastomeric phase with stable morphology and good properties of the blends is achieved, even at a relatively high proportion of elastomeric phase.[16]

A large number of elastomers/thermoplastics blends have been introduced with dynamic vulcanization, such as ethylene-propylene-dieneterpolymer (EPDM)/polypropylene (PP), nitrile butadiene rubber (NBR)/poly(vinyl chloride) (PVC), NBR/polyamide (PA), natural rubber/PP and so on.[17-19] Recently, there have been numerous reports on PVDF blends and various amorphous polymers, including poly(vinyl fluoride) (PVF), poly(methyl methacrylate) (PMMA), poly(vinyl pyrrolidone) (PVP), poly(3-hydroxy butyrate) (PHB), and *etc*. However, there are few reports about the dynamic vulcanization of PVDF/rubber blends.[20-22] Physically cross-linked rubber-like materials are referred to as "thermoplastic elastomers" (TPE), since they possess processing properties of thermoplastics and the elastomeric properties of the thermoset elastomers. A TPE is mainly achieved by the synthesis of a block copolymer or by dynamic vulcanization plastic/rubber blend.[23,24] A large number of thermoplastics and elastomers have been introduced in order to produce thermoplastic vulcanizates by dynamic vulcanization, for example, nitrile rubber (NBR)/(PVDF),[16] NBR/polyamide (PA),[25] natural rubber/polypropylene (PP),[26] and ethylene-propylene-dieneterpolymer (EPDM)/PP,[27] SR/PVDF.[15]

In this study employing bisphenol A, as a curing agent, we have produced PVDF/FKM blends with and without curing system. The effect of curing agent was studied in detail on morphology, thermal, mechanical, and dynamic mechanical properties of the blends. The selected FKM and PVDF have the same elemental chain constituents with better compatibility.

Experimental

Materials. PVDF (Hylar 460) with excellent temperature resistance and high chemical stability was purchased from Solvay Solexis (United States). Viton-A100 was purchased from DuPont (United States). This is normally blended with other fluorine family types to enhance processibility and flowability. Viton-A100 is an uncured category of FKM. This grade of FKM is strongly resistant to wide range of oils, fuels, lubricants. Another FKM type in this work was the Viton-A401C which is included MgO (3 phr) as stabilizing agent and $Ca(OH)_2$ (6 phr) as acid acceptor agent to absorb hydrogen fluoride generation by bisphenol A (1 phr) as curing agent. This grade of FKM material which was also purchased from DuPont (United States) has high compression set resistance as its main property.

Compositions and Sample Preparation. The PVDF/FKM blends were prepared in an internal mixer (Brabender W50EHT, Germany) by mixing the components in the molten state at 170 °C and rotor speed of 90 rpm. The mechanism for crosslinking-controlled core–shell structures is shown in Figure 1.

In torque profiles, the first peak corresponded to the introduction of PVDF into the mixer, and the second peak corresponded to FKM loading. An increase of torque was observed when the highly viscous FKM was added. Bisphenol

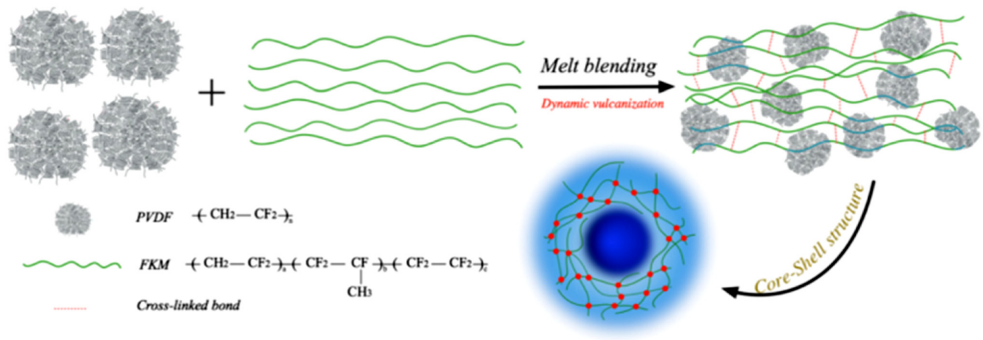

Figure 1. Mechanism for cross-linked reaction of PVDF/FKM blends.

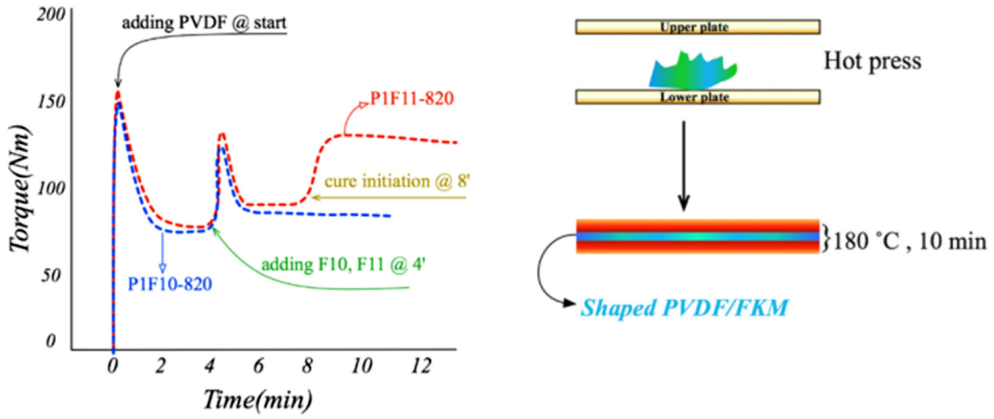

Figure 2. Torque-time during mixing of PVDF/FKM blends.

A caused a sudden increase in torque, which was related to the drastic changes in the viscosity and elasticity of the FKM phase due to cross-linked. According to Figure 2, PVDF was first shear-melted in 4 min, and when the FKM compound was added it was mixed for another 8 min. The blends were removed from the mixer and cooled to room temperature. Then, the lump-shaped samples were chopped into small gran for easy compression molding. The test specimens were compressed at 180 ºC and 10 min by hot press molding.

Dynamically vulcanized and uncured blends were selected with PVDF/FKM weight ratios of 90/10, 80/20, 70/30 and 60/40. Different weight ratios of bisphenol A as curing agent were taken to maintain a constant concentration relative to the amount of FKM. The compositions in terms of the components weight ratios for PVDF/FKM blends are presented in Table 1.

Table 1. Formulation of the Prepared Samples (weight ratio by wt%)

Sample code	FKM	PVDF	Bisphenol A
P1	0	100	-
F10	100	0	-
F11	100	0	1
P1F10-910	10	90	-
P1F10-820	20	80	-
P1F10-730	30	70	-
P1F10-640	40	60	-
P1F11-910	10	90	0.1
P1F11-820	20	80	0.2
P1F11-730	30	70	0.3
P1F11-640	40	60	0.4

Thermal Analysis. DSC: Melting and crystallization of the blends were measured under nitrogen atmosphere using a Perkin Elmer differential scanning calorimeter (Pyris, UK). For each test, 5-6 mg sample was first heated to 250 ºC at a rate of 10 ºC/min and kept at this temperature for 5 min to eliminate previous thermal history of the blend. The sample was cooled to room temperature at a cooling rate of 20 ºC/min and reheated to 250 ºC at the same heating rate (ASTM D 3418).

TGA: A Perkin Elmer thermogravimeter (Pyris, UK) was used to measure the weight loss of the blends under nitrogen atmosphere. The samples were heated from ambient temperature up to 600 ºC at a heating rate of 20 ºC/min. Approximately 10 mg of sample was used in each analysis (ASTM E 1131).

Tensile Properties Measurements. Standard tensile tests were conducted on dumbbell shaped specimens using a universal testing instrument (GoTech, China) with a tensile mode at room temperature. Test speed was kept at 50 mm/min, according to ASTM D638. All the above tests were repeated on at least five test pieces, and the results were reported as average.

Dynamic Mechanical Analysis. Dynamic mechanical properties were evaluated using a dynamic mechanical analyzer in single cantilever bending mode (ASTM E1640) at a frequency of 1 Hz, constant strain of 0.02 and in the temperature range of -100 ºC to 120 ºC at a heating rate of 5 ºC/min by Tritec 2000, DMTA-Triton, England.

Rheological Characterization. Rheological properties of the blends were investigated using a rheometric mechanical spectrometer (RMS) equipped with parallel plate geometry (diameter=25 mm, gap=1 mm). The frequency sweep tests were performed in the range of 0.1-600 s^{-1} at temperature of

180 °C and with amplitude of 3% in order to maintain the response of materials in a linear viscoelastic regime.

Results and Discussion

Thermal analysis. TGA: The thermal stability of the PVDF/FKM blends was evaluated under nitrogen atmosphere through the weight loss using TGA. The main PVDF degradation occurred at about 460 °C, indication of an excellent thermal stability, whereas the main FKM degradation occurred between 350 and 460 °C. As shown in Figure 3, the thermogram of P1 and F11 showed a typical single degradation step profile. The temperature for 10% weight loss for the neat PVDF and F11 were 456 and 405 °C, respectively. Incorporation of FKM obviously lowered the onset decomposition temperature of the PVDF phase. However, no distinct degradation stage of FKM was found in TGA curves of the cured PVDF/FKM blends, which indicated that the crosslinked F11 particles had been completely covered by the PVDF molecules through good interfacial interactions.

At higher FKM content, degradation temperature of the blends is decreased due to low degradation temperature of FKM (405 °C), and the mass of residue at 600 °C decreased by adding FKM. It should be noted that due to the high PVDF thermal resistance and its good mixing and interaction with FKM molecular chains, the latter had little effect on thermal resistance of the whole system. The results are summarized in Tabel 2.

DSC: The melting curves of PVDF/FKM blends are shown in Figure 4. As seen in this figure, the T_m shifted to higher temperature after blending with FKM. The sharp melting peak which is located and detected at about 167 °C corresponds to the melting of PVDF. No melting and crystallization peaks are observed for neat FKM due to its amorphous nature. The viscosity of the blends dropped when the FKM content was increased, suggesting that motion and folding of the PVDF molecular chains were promoted. By addition of F10 the melting temperature was raised from 166.6 to 168.8. By addition of F11 the melting temperature increased from 166.6 to 172.4. The rise of 10% by weight of F10 raised the melting temperature by less than 1 °C. Increases in F10 (30-40 wt%) it had little small on the melting temperature, while increases of F11 by the same amount increased the melting temperature of the blend by about 6 °C, because of increased network density and decreased polymer chain movement.

Table 2. TGA Parameters in PVDF/FKM Blends

Sample	Temperatures @10% weight loss (°C)	Mass of residual (%)
P1F10-910	444	29.2
P1F10-820	441	28.5
P1F10-730	439	27.1
P1F10-640	437	26.1
P-F11-910	447	25.5
P1F11-820	444	24.6
P1F11-730	440	22.8
P1F11-640	439	23.2
P1	456	20.5
F11	405	34.2

The non-isothermal crystallization curves of the blends are shown in Figure 5. As shown in this figure, the incorporation of high molecular weight PVDF shifts the crystallization temperature of PVDF upwards. The rubber network may retard the formation of full and large PVDF crystals because the PVDF molecular chains were separated by the FKM particles.

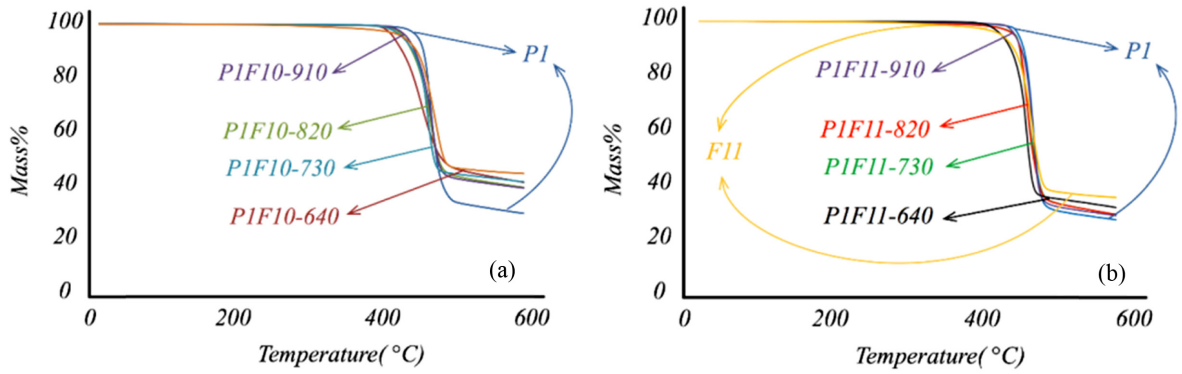

Figure 3. TGA curves of (a) uncured; (b) dynamically vulcanized PVDF/FKM blends.

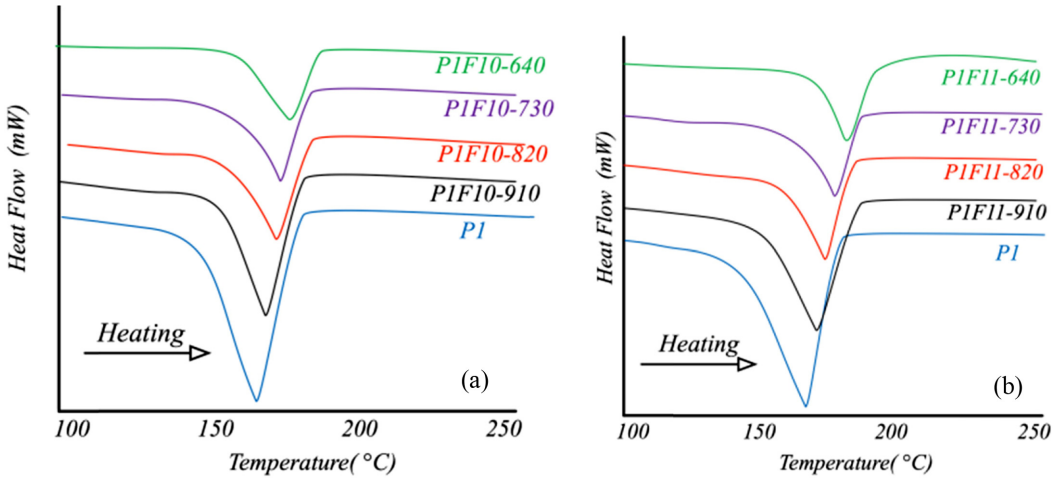

Figure 4. Calorimetric melting curves of PVDF/FKM blends (heating rate V_h=10 °C min^{-1}): (a) uncured; (b) dynamically vulcanized.

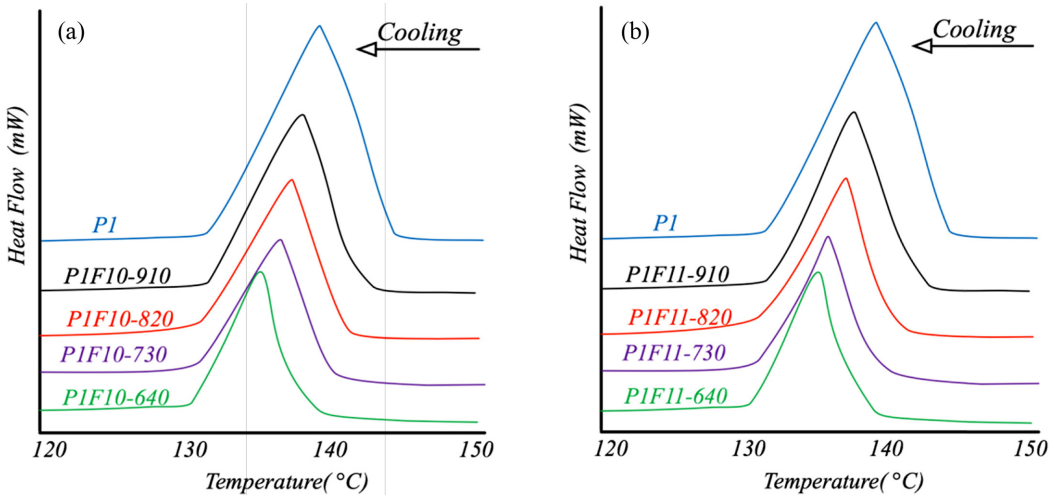

Figure 5. Crystallization curves of PVDF/FKM blends of different compositions (cooling rate V_c=10 °C min^{-1}): (a) without curing agent; (b) with curing agent.

The PVDF total crystallinity X_c was calculated by:[28]

$$X_c = \frac{\Delta H_c^* *}{\Delta H_c \varphi} \times 100\% \quad (1)$$

Where ΔH_c^* = 104.7 J/g, is the melting enthalpy for a 100% crystalline PVDF, φ is PVDF weight fraction of blends and ΔH_c is the melting enthalpy of PVDF measured in DSC.

The FKM effect before and after curing (F10, F11), in the blends on the crystallization peak temperature (T_c) and the melting temperature (T_m) is summarized in Table 3. The viscosity of the blends is dropped with higher FKM content, suggesting that motion and folding of the PVDF molecular chains has been promoted. The T_c has also decreased with increases in FKM content (Figure 5). The crystallization peak of the blends

Table 3. Melting Enthalpy (ΔH_c), Crystallinity (X_c), Melting Temperature (T_m) and Crystallization Peak Temperature (T_c) of PVDF/FKM blends

Sample code	ΔH_c (J/g)	X_c (%)	T_m (°C)	T_c (°C)
P1F10-910	42.47	45.1	167.2	138.9
P1F10-820	39.18	41.6	167.5	138.6
P1F10-730	29.09	39.7	168.1	138.4
P1F10-640	23.99	38.2	168.8	137.2
P1F11-910	43.62	46.3	167.1	138.6
P1F11-820	36.77	43.9	168.4	138.5
P1F11-730	31.07	42.4	172.2	138.1
P1F11-640	25.19	40.1	172.4	137.6
P1	53.61	51.2	166.6	139.1

has moved to lower temperature, suggesting that FKM could have acted as an effective nucleation agent, accelerating the crystallization of PVDF in the blends. Seen from Figure 4, T_m degrees of all samples show no obvious changes and they are maintained at around 167 °C.

The melting temperature of PVDF in the blends is slightly lower than that of pure PVDF due to lower crystallinity. By addition of F10 and F11 (FKM before and after curing) into blend samples, the crystallization temperature is reduced by less than 2 °C by breaking PVDF crystals and reducing the crystallization temperature. On the other hand, because of FKM nucleation effect the crystallization temperature is increased and so it prevents a much change in the crystallization temperature.

Tensile Properties. The tensile properties of the blends are shown in Figure 6. Neat PVDF is a semi-crystalline polymer having low elongation-at-break of about 13%. It is evident that the material reaches its yielding point without necking. The addition of FKM has significantly lowered the yield stress, arising from smaller content of PVDF continuous phase and softening of the blends. It is very interesting to note that a broad plateau of stress is obtained when the strains pass the yield point for the cured PVDF/FKM blends. Interfacial adhesion between the PVDF and FKM phases is a key factor to increase elongation-at-break. The detailed tensile properties of the blends are shown in Table 4. When the stress was transferred from the PVDF matrix to the rubber phase, the cross-linked network of the rubber phase could effectively transfer the stress more uniformly.

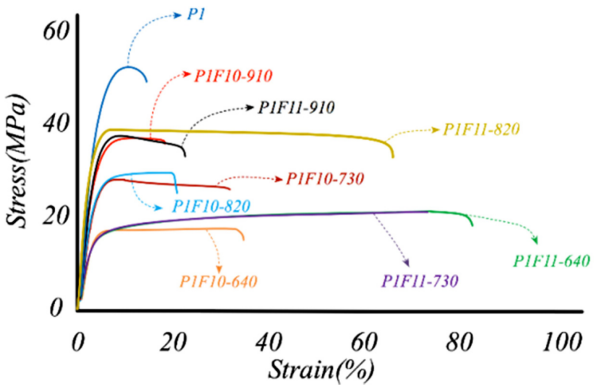

Figure 6. Tensile stress-strain curves for PVDF/FKM blends with/without curing agent.

Subjecting to a stress, the F11-shell could act as an effectual transition layer while the F10 might be easily damaged resulting in an early end of stress-transfer. In addition, F11 had a higher strength to bear stress and dissipate the energy, which contributed to the mechanical properties of the TPVs. In presence of curing agent, the modulus of 100% in P1F11-910 containing a low FKM percentage is increased, but at higher rubber content in samples P1F11-820, P1F11-730, P1F11-640, this behavior is completely reversed, due to the formation of matrix morphology the surface tension between the cured FKM and PVDF is reduced.

Dynamic Mechanical Properties. Figure 7 show the temperature dependence of tan δ of the uncured and dynamically vulcanized PVDF/FKM blends on different compositions. In particular, a significant modulus drop was found when the FKM concentration was increased. Two distinct tan δ peaks corresponding to the glass transition temperatures of PVDF and FKM can be observed in all blends. The temperature at around -29 °C is related to the glass-rubber transition of the PVDF phase and the other at around -5 °C corresponds to the transition of the FKM phase, and their intensities are pro-

Table 4. Tensile Properties of Dynamically Vulcanized PVDF/FKM Blends

Sample	Modulus (MPa)	Elongation-at-break (%)	Tensile strength (MPa)
P1F10-910	7.6(±0.1)	20.5(±0.1)	36.8(±0.6)
P1F10-820	7.3(±0.1)	30.2(±0.2)	31.1(±0.3)
P1F10-730	6.4(±0.2)	35.6(±0.2)	22.3(±0.4)
P1F10-640	4.5(±0.3)	38.9(±0.3)	18.4(±0.6)
P1F11-910	8.1(±0.1)	25.3(±0.1)	37.9(±0.5)
P1F11-820	6.9(±0.2)	67.5(±0.2)	32.7(±0.6)
P1F11-730	3.8(±0.2)	78.4(±0.2)	23.4(±0.4)
P1F11-640	3.7(±0.3)	83.6(±0.4)	21.2(±0.5)
P1	11.3(±0.1)	13.5(±0.1)	51.5(±0.7)
F11	0.01(±0.002)	589(±1.4)	6.3(±0.4)

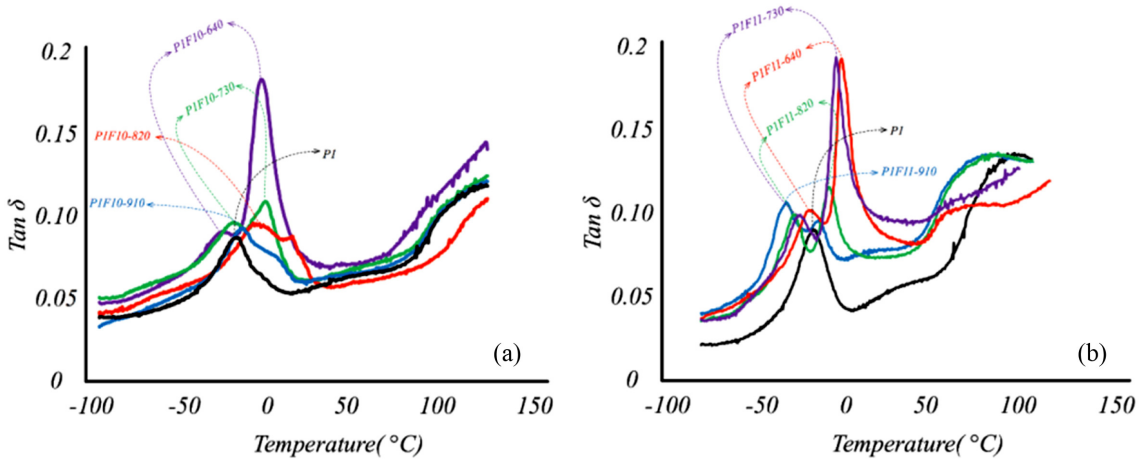

Figure 7. Tan δ profiles for (a) uncured; (b) dynamically vulcanized PVDF/FKM blends.

Table 5. Tan δ Peak Temperature (°C) of the FKM and PVDF Phase

Sample code	PVDF phase	FKM phase
P1	-29	-
F11	-	-5
P1F10-910	-28.6	-
P1F10-820	-26.3	-13.1
P1F10-730	-27.1	-10.5
P1F10-640	-28.4	-7.6
P1F11-910	-27.7	-6.4
P1F11-820	-27.1	-4.3
P1F11-730	-25.6	-3.1
P1F11-640	-25.2	-3.5

portional to the relative fractions in the blends. The results of tan δ peak temperature summarized in Table 5.

Tan δ peak temperature of the FKM phase was increased but that of PVDF was kept almost constant. It is well known that a higher cross-link density results at higher tan δ peak temperature of cross-linked rubber, and thus the increased tan δ peak temperature of F11 phase obviously resulted from an increased cross-link density due to the relative increase of bisphenol A, and thus decreasing the mobility of F11chains considerably.

At the same time, the higher crosslink density improved the mechanical properties of the cross-linked FKM particles. The entanglement between F11 particles was improved by shortening the distance between these particles, resulting in improved properties of the blends.

Morphology and Rheology and Analysis. The morphology structure of the crosslinked core/shell particles was observed by SEM. The fracture surfaces of TPVs have been etched by hot *N,N*-dimethylformamide (DMF) to remove away the PVDF. The result of P1F11-640 is shown in Figure 8. The SEM images reveal that the cross-linked rubber phases are presented in spherical particles which are uniformly distributed in the PVDF matrix.

The storage modulus (G') and complex viscosity (η^*), as a function of frequency, for two different PVDF/FKM blends are presented in Figure 9. The storage and loss modulus of PVDF/FKM blends keep increasing with frequency. In contrast to G', no plateau exists in the log loss modulus G'' versus log frequency curve. For all samples, a power law behavior for G'', with exponents smaller than 1, can be observed at low frequency. This might be ascribed to proper interaction and entanglement between FKM molecules and PVDF molecules and fine dispersion of the rubber particles.

The values of G' and G'' decrease with increasing weight content of PVDF over the whole range of frequencies investigated. Here, we apply the generalized Maxwell models to study the rheology of the compatibilized PVDF/FKM blends.

The generalized Maxwell model may be used to model viscoelastic behavior when no long term limitation of compliance is apparent, i.e., either terminal behavior or the high frequency tail of any transition.[28]

The most popular approach to describe the behavior of polymer melts in linear viscoelastic experiments is a generalized Maxwell model. The function used in this model is:

$$G(t-t')=\Sigma G_k \exp[-(t-t')/\lambda_k] \quad (2)$$

Where, G_k is the relaxation modulus, λ_k is the relaxation time,

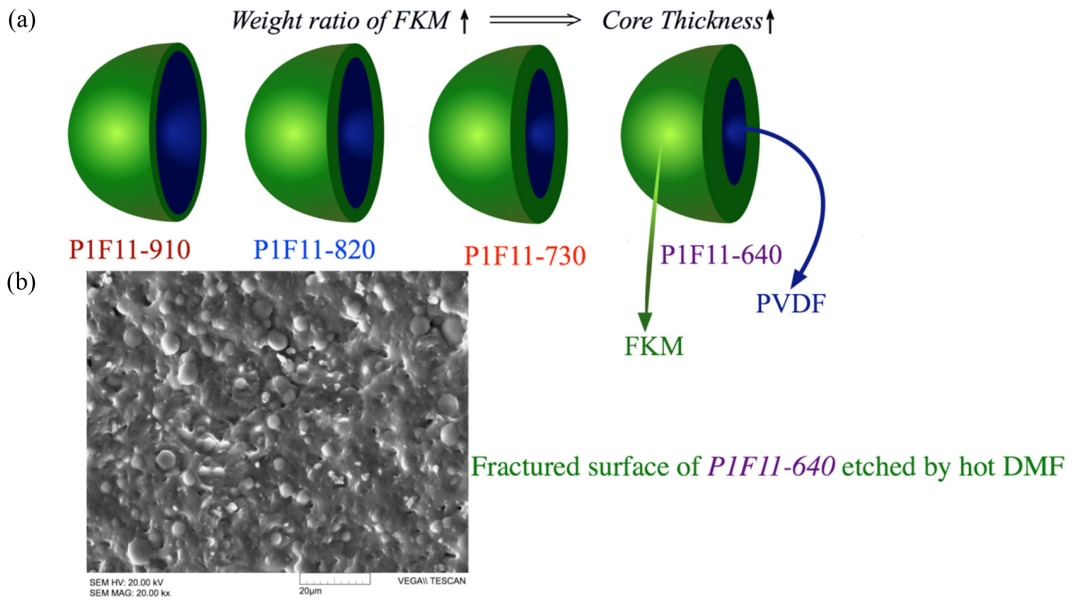

Figure 8. (a) Schematic presentation of the core-shell structure in PVDF/FKM TPV; (b) DMF-etched surface morphology of the blend (P1F11-640).

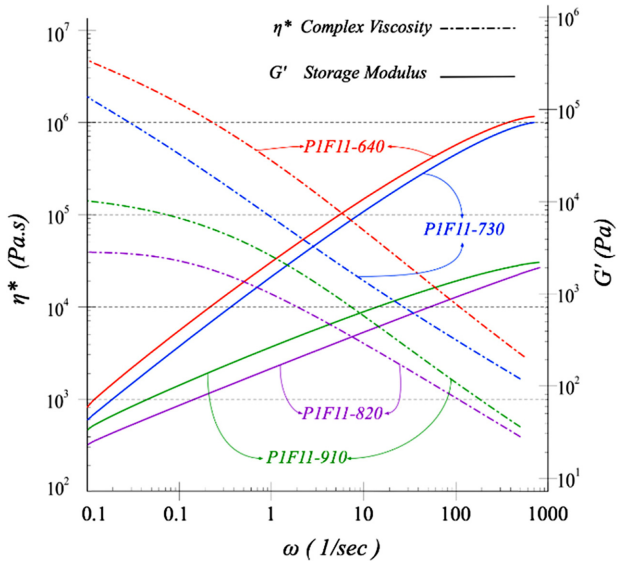

Figure 9. Storage modulus (G') and complex viscosity (η^*) versus frequency profiles for PVDF/FKM blend at 180 °C.

and k is the discrete experimental data. From oscillatory shear experiments, the model parameters (G_k, λ_k, and η_k) can be determined using the following eq. (3)-(6):

$$G'(\omega) = \sum_k G_k \frac{\omega^2 \lambda_k^2}{1+\omega^2 \lambda_k^2} \tag{3}$$

$$G''(\omega) = \sum_k G_k \frac{\omega^2 \lambda_k^2}{1+\omega^2 \lambda_k^2} \tag{4}$$

$$\eta'(\omega) = \sum_k \frac{\eta_k}{1+\omega^2 \lambda_k^2} \tag{5}$$

$$\frac{\eta''(\omega)}{\omega} = \sum_k \frac{\eta_k \lambda_k}{1+\omega^2 \lambda_k^2} \tag{6}$$

The term win the expressions given, refers to experimental frequencies. In this study the linear least-square method was used to obtain the relaxation time and the viscosity index. For five sets of experimental range of frequencies, the model parameters (λ_k and η_k) were calculated using the eq. (5) and the experimental sets of data. For this purpose, the eq. (5) was re-written as follows:

$$\frac{1}{\eta'(\omega)} = \frac{1}{\eta_k} + \frac{\lambda_k^2}{\eta_k}\omega^2 \tag{7}$$

This equation can be written as:

$$Y = A + BX \tag{8}$$

Where, $Y = \frac{1}{\eta'(\omega)}$, $A = \frac{1}{\eta_k}$, $X = \omega^2$, $B = \frac{\lambda_k^2}{\eta_k}$

Thus, relation between $1/\eta'(\omega)$ and ω^2 can be found with splitting into various limited ranges of frequencies and $1/\eta'(\omega)$ versus ω^2 at each temperature plotted. The values of parameters which were obtained using this method are in a good agreement with the experimental $\eta'(\omega)$ data. The results sum-

Table 6. Values of *A* and *B* in *Y=A+BX* of Eq. (8) and *R* Squared after Linear Interpolation

Sample code / ω (rad/s)	P1F11-910			P1F11-820			P1F11-730			P1F11-640		
	A	*B*	R^2	*A*	*B*	R^2	*A*	*B*	R^2	*A*	*B*	R^2
0.000175-0.000991	5×10^{-7}	1.1×10^{-1}	0.97	3×10^{-7}	9.5×10^{-2}	0.96	4×10^{-8}	6.37×10^{-2}	0.94	4×10^{-8}	4.2×10^{-2}	0.94
0.01763-0.010053	7×10^{-7}	4.9×10^{-3}	0.94	5×10^{-7}	3.8×10^{-3}	0.94	2×10^{-7}	2.6×10^{-3}	0.95	1×10^{-7}	1.7×10^{-3}	0.95
0.017977-0.101927	2×10^{-6}	2×10^{-4}	0.94	1×10^{-6}	2×10^{-4}	0.95	7×10^{-7}	1×10^{-4}	0.96	5×10^{-7}	9×10^{-5}	0.96
0.181514-1.03323	6×10^{-6}	8×10^{-6}	0.95	5×10^{-6}	7×10^{-6}	0.95	4×10^{-6}	7×10^{-6}	0.95	2×10^{-6}	5×10^{-6}	0.95
1.85005-10.47198	2×10^{-5}	5×10^{-7}	0.96	2×10^{-5}	4×10^{-7}	0.96	2×10^{-5}	4×10^{-7}	0.97	1×10^{-5}	3×10^{-7}	0.96

Table 7. η_k and λ_k in Maxwell Model of Eq. (7) at Four Different Samples

Sample code / ω (rad/s)	P1F11-910		P1F11-820		P1F11-730		P1F11-640	
	η_k	λ_k	η_k	λ_k	η_k	λ_k	η_k	λ_k
0.000175-0.000991	2×10^{6}	4.7×10^{2}	3.3×10^{6}	5.6×10^{2}	2.5×10^{7}	1.26×10^{3}	2.5×10^{7}	1×10^{3}
0.017628-0.100529	1.7×10^{6}	9.1×10^{1}	2×10^{6}	8.7×10^{1}	5×10^{6}	1.14×10^{2}	1×10^{7}	1.4×10^{2}
0.01763-0.010053	5×10^{5}	1×10^{1}	1×10^{5}	4.47×10^{0}	1.7×10^{6}	1.3×10^{1}	2×10^{6}	1.3×10^{1}
0.181514-1.03323	1.6×10^{4}	1.13×10^{0}	2×10^{5}	1.18×10^{0}	2.5×10^{5}	1.32×10^{0}	5×10^{5}	1.5×10^{0}
1.85005-10.47198	5×10^{4}	1.6×10^{-1}	5×10^{4}	1.4×10^{-1}	5×10^{4}	1.41×10^{-1}	1×10^{5}	1.7×10^{-1}

marized in Table 6 are after calculating the A and B in eq. (8). The parameters of GMM are then obtained. Table 7 shows the GMM parameters which were determined from Table 6 at temperatures of 180 °C.

Conclusions

PVDF/FKM blends with different compositions were prepared by bisphenol A dynamic vulcanization. Incorporation FKM decreased the tensile strength and increased their elongation-at-break, increased the availability of bisphenol A in FKM phase during mixing and increasing its crosslink density. This resulted in shifting the tan δ of FKM phase in the blend to higher temperature, whereas that of the PVDF phase remained almost unchanged. Interestingly, the residual mass of the blends was much higher than that of pure PVDF and F11 values. All the results indicated that good interfacial interaction was achieved between PVDF continuous phase and FKM dispersed phase.

A method based on the generalized Maxwell model was used to calculate η_k and λ_k. The results showed that η_k, a characteristic of viscosity, was decreased with increasing temperature and frequency due to lowered viscosity. As λ_k, the relaxation time, was decreased with the increase of temperature and frequency, it can be concluded that these material functions are related to the rubber chain mobility.

References

1. E. Sharifzadeh, I. Ghasemi, M. Karrabi, and H. Azizi, *Iran. Polym. J.*, **23**, 525 (2014).
2. H. Ma, Z. Xiong, F. Lv, C. Li, and Y. Yang, *Macromol. Chem. Phys.*, **212**, 252 (2011).
3. A. Fina, Z. Han, G. Saracco, U. Gross, and M. Mainil, *Polym. Adv. Technol.*, **23**, 1572 (2012).
4. S. Mohamadi and N. Sharifi-Sanjani, *Polym. Composite*, **32**, 1451 (2011).
5. S. H. Lin, C. F. Hsieh, M. H. Li, and K. L. Tung, *Desalination*, **249**, 647 (2009).
6. Z. Major and R. W. Lang, *Eng. Fail. Anal.*, **17**, 701 (2010).
7. S. H. Lee, S. S. Yoo, D. E. Kim, B. S. Kang, and H. E. Kim, *Polym. Test.*, **31**, 993 (2012).
8. K. P. Pramoda, N. T. T. Linh, P. S. Tang, and W. C. Tjiu, *Compos. Sci. Technol.*, **70**, 578 (2010).
9. C. Zhao, X. Xu, J. Chen, G. Wang, and F. Yang, *Desalination*, **340**, 59 (2014).
10. M. A. Rahman and G. S. Chung, *J. Alloy Compd.*, **581**, 724 (2013).
11. X. Kuang, Q. Gao, and H. Zhu, *J. Appl. Polym. Sci.*, **129**, 296 (2013).
12. J. Gao, Z. Gu, G. Song, P. Li, and W. Liu, *Appl. Clay Sci.*, **42**, 272 (2008).
13. N. Hinchiranan, P. Wannako, and B. Paosawatyanyong, *Mater. Chem. Phys.*, **139**, 689 (2013).
14. M. A. Kader, M. Y. Lyu, and C. Nah, *Compos. Sci. Technol.*, **66**, 1431 (2006).

15. Y. Wang, X. Jiang, C. X, Z. Chen, and Y. Chen, *Polym. Test.*, **32**, 1392 (2013).
16. C. Xu, Y. Wang, and Y. Chen, *Polym. Test.*, **33**, 179 (2014).
17. K. Ke, Y. Wang, W. Yang, B. H. Xie, and M. B. Yang, *Polym. Test.*, **31**, 117 (2012).
18. N. Wang, P. R. Chang, P. Zheng, and X. Ma, *Appl. Surface Sci.*, **314**, 815 (2014).
19. R. D. Simoes, A. E. Job, D. L. Chinaglia, V. Zucolotto, J. C. Camargo-Filho, N. Alves, J. A. Giacometti, and O. N. Oliveira, *J. Raman Spectrosc.*, **36**, 1118 (2005).
20. A. S. Bhatt, D. K. Bhat, and M. S. Santosh, *J. Appl. Polym. Sci.*, **119**, 968 (2011).
21. D. Bhadra, M. G.Masud, S. Sarkar, J. Sannigrahi, S. K. De, and B. K. Chaudhuri, *J. Polym. Sci.; Part B: Polym. Phys.*, **50**, 572 (2012).
22. I. H. Kim, D. H. Baik, and Y. G. Jeong, *Macromol. Res.*, **20**, 920 (2012).
23. H. Ma, Z. Xiong, F. Lv, C. Li, and Y. Yang, *Mater. Sci. Eng.*, **297**, 136 (2012).
24. M. M. Abolhasani, A. Jalali-Arani, H. Nazockdast, and Q. Guo, *Polymer*, **54**, 4686 (2013).
25. Y. Wang, L. Fang, C. Xu, Z. Chen, and Y. Chen, *Polym. Test.*, **32**, 1072 (2013).
26. L. Valentini, A. Bolognini, A. Alvino, S. B. Bon, and M. Martin-Gallego, *Composites: Part B*, **60**, 479 (2014).
27. W. Z. Zhang, J. Wang, and X. L. Wang, *Appl. Surface Sci.*, **253**, 8377 (2007).
28. J. Varga and A. Menyhárd, *J. Therm. Anal. Calorim.*, **73**, 735 (2003).